Journal of Power Sources 187 (2009) 25–31

Contents lists available at ScienceDirect

Journal of Power Sources

journal homepage: www.elsevier.com/locate/jpowsour

Compositional influence of LSM-YSZ composite cathodes on improved performance and durability of solid oxide fuel cells

Hwa Seob Song[a], Seungho Lee[a], Sang Hoon Hyun[a], Joosun Kim[b], Jooho Moon[a,*]

[a] Department of Materials Science and Engineering, Yonsei University, Seoul 120-749, Republic of Korea
[b] Center for Energy Materials Research, Korea Institute of Science and Technology, Seoul 136-791, Republic of Korea

ARTICLE INFO

Article history:
Received 14 July 2008
Received in revised form 21 August 2008
Accepted 14 October 2008
Available online 6 November 2008

Keywords:
Solid oxide fuel cell
Composite cathode
Durability
Dual composite

ABSTRACT

The use of a dual-composite approach, in which both LSM and YSZ nanoparticles are placed on YSZ core particles, allows for the development of an ideal cathode microstructure with improved phase contiguity and durability for use in solid oxide fuel cells. The volume fraction of the conjugated YSZ phase plays a critical role in the optimization of the cathode microstructure for achieving good durability because it acts as an interconnecting bridge between YSZ core particles. However, the presence of excess conjugated YSZ phase interrupts the formation of sufficient triple phase boundary sites by disturbing the contacts between the LSM and YSZ phases. Impedance spectroscopy analysis and microstructural observations provide a better understanding of the influence of the composition on the electrochemical performance and durability of these dual composite cathodes.

1. Introduction

Solid oxide fuel cells (SOFCs) can provide high efficiency energy conversion because of their high operation temperatures, ~800 °C [1]. For the practical use of SOFCs, it is essential to achieve not only higher performance but also long-term stability, i.e., over 10,000 h at high temperature. There are several possible cathode degradation mechanisms. For instance, inhomogeneous current distribution over the cathode, which causes local current density overload, can lead to microstructural degradation and compositional changes via grain growth, chemical reactions, and delamination [2–4]. In addition, the stability of the cathode|electrolyte interface plays an important role in minimizing electrode polarization [5,6]. It is well known that $La_2Zr_2O_7$ formation between $La_{1-x}Sr_xMnO_3$ (LSM) and yttria stabilized zirconia (YSZ) particles increases the polarization resistance. However, the degradation mechanism itself is not yet clearly understood, especially for nanostructured cathodes. A nanoporous cathode is expected to exhibit a lower cathodic overpotential because of its large effective surface area for electrocatalytic reactions. Unfortunately, such nanoporous electrodes are generally vulnerable to degradation at high temperatures, but demonstrate excellent short-term cell performance [4].

One of the approaches to generate durable electrodes is to form a nanoporous skeleton of an ionic conduction phase first and then to infiltrate this skeleton with a salt solution of the electronic conduction phase. However, the infiltration procedure is time-consuming, and it is difficult to achieve a uniform distribution of the infiltrated phase over the skeleton by infiltration [7]. In previous work, we introduced engineered nanocomposite particles to produce a highly durable, LSM–YSZ, dual composite cathode (LYDC). The use of this dual-composite approach, in which both LSM and YSZ phases are placed on a YSZ core as shown in Fig. 1, allows for the development of an ideal cathode microstructure with improved phase contiguity and interfacial coherence.

In the present work, we have investigated the influence of the composition of the cathode, such as the ratio of surface conjugated YSZ to YSZ core particles, on the long-term durability of the cathode. The conjugated YSZ component plays critical roles in constructing a strong YSZ skeleton and in creating sufficient triple phase boundary (TPB) sites by interacting with the LSM component. Variation of the composition of the dual composite cathode enables long-term electrochemical activity through optimization of the microstructure of the composite cathode.

2. Experimental

The LSM ($La_{0.7}Sr_{0.3}MnO_3$)–YSZ (Tosoh TZ8Y, surface area = 12.74 $m^2\,g^{-1}$, mean particle size = 78 nm) composite powder was prepared via the polymerizable complex method [8,9]. The experimental procedure is described in detail in our previous work

* Corresponding author. Tel.: +82 2 2123 2855 fax: +82 2 365 5882.
E-mail address: jmoon@yonsei.ac.kr (J. Moon).

0378-7753/$ – see front matter © 2008 Elsevier B.V. All rights reserved.
doi:10.1016/j.jpowsour.2008.10.092

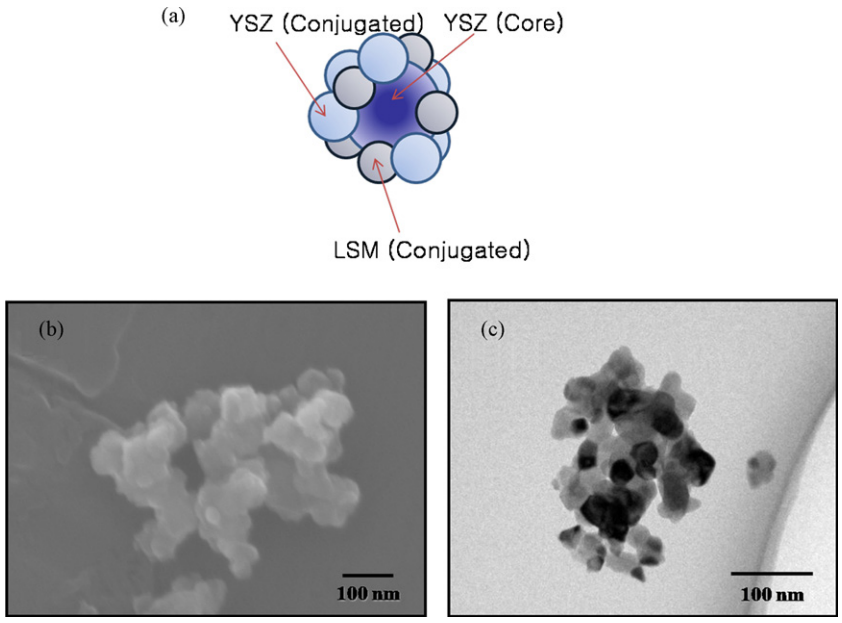

Fig. 1. LSM–YSZ dual composite particles: (a) schematic representation, (b) SEM image, (c) TEM image.

[10]. The YSZ core particles were suspended in polymeric resin obtained by esterification between the metal ions (La, Sr, Mn, Y, and Zr), organic complex, and ethylene glycol. Upon calcination at 1000 °C for 2 h, the surrounding polymeric resin was transformed into the LSM and YSZ phases conjugated on the YSZ core particles. The resulting LYDC consisted of LSM and YSZ nanoparticles of approximately 30–50 nm in size attached to the YSZ core particles. LYDCs with four different compositions were prepared by varying the LSM:YSZ ratio. The portion of conjugated YSZ with respect to the YSZ core varied from 5 to 30 vol%. We denote the LYDC with a ratio of 47:42:11 vol% of conjugated LSM:YSZ core:conjugated YSZ as LYDC 47-42-11. The volume ratio of LSM to YSZ is one of the important factors that determine the electrocatalytic performance of the composite cathode because the formation of both TPB sites and ionic/electronic conduction pathways can be influenced by cathode composition. The volume ratio of LSM:YSZ was fixed at 47:53 for the LYDCs. By contrast, a cathode derived from mechanically mixed, submicrometer-sized particles at a lower YSZ volume fraction (LSM:YSZ = 57:43) demonstrated a lower polarization resistance (0.35 $\Omega\,cm^2$) in our previous report. [11] This observation indicates that there exists an optimum LSM:YSZ ratio that depends on the mixing order as well as on the structure and relative size ratio of the starting particles.

Four symmetrical cells (LSM–YSZ/YSZ/LSM–YSZ), using composite cathodes of LYDCs 47-48-5, 47-42-11, 47-32-21, and 47-23-30, were constructed. The cathode layers were deposited on a YSZ disc (sintered at 1400 °C for 4 h, thickness = 0.5 mm, diameter = 20 mm) by screen-printing and sintered at 1100 °C for 4 h. The area of the applied cathode was 1.4 cm^2 and the thickness was about 25–30 μm. Electrochemical impedance measurements were performed on the symmetrical cells under various oxygen partial pressures using a.c. impedance spectroscopy (Solatron SI 1260/1287) [12–15]. Impedance spectra were obtained in a frequency range from 100 kHz to 0.1 Hz with an applied a.c. voltage amplitude of 20 mV.

A NiO-YSZ anode-supported cell involving the composite cathode was also fabricated. The NiO-YSZ anode supports were prepared by pressing the polymeric resin-derived nanocomposite powders.[9] A YSZ electrolyte of 6–7 μm in thickness was placed on the anode support via the dip-coating method. After sintering at 1400 °C for 4 h, one side of the support was polished to remove the YSZ electrolyte and to adjust the anode support thickness to ~1.0 mm. Platinum mesh and nickel felt were used as a current collector on the cathode and anode layers, respectively. Full-cell performance was investigated using humidified hydrogen as fuel and air as the oxidant at ambient pressure and 800 °C. The flow rate for the hydrogen and air was 200 and 250 sccm, respectively. A pyramid-type cyclic current load was used for accelerated lifetime tests (ALT) for both half- and full-cells. While applying such a current load, impedance spectra and power density (at 0.7 V) data were recorded.

The cross-sectional microstructures of the polished composite cathodes before and after LSM etching were investigated by means of field emission scanning electron microscopy (FE-SEM, JSM 6700F, JEOL). For analysis of the YSZ phase contiguity, the LSM phase was dissolved by hydrochloric acid treatment, followed by backscattering image analysis to generate YSZ/pore binary images from which phase contiguity was calculated via image analysis [16].

3. Results and discussion

Electrochemical impedance spectroscopy (EIS) is a suitable method for investigating the kinetics and activity of an electrochemical reaction. Interfacial polarization resistances in electrochemical cells can be resolved into elementary reaction steps to provide a better understanding of the electrode processes. Previously, we demonstrated that the impedance spectra for LSM–YSZ cathodes fit well to a model with two major arcs, denoted *process A* (high frequency) and *process B* (low frequency). It was recognized that the resistance for *process A* (R_A) is related to the YSZ phase interconnectivity whereas that for *process B* (R_B) reflects the TPB site density [10,11].

Fig. 2 shows the interfacial polarization resistances, together with the total and resolved (*process A* and *process B*) resistances for cells with four different LSM–YSZ compositions. The LYDC 47-48-5 cathode exhibit the lowest resistance (0.385 $\Omega\,cm^2$), whereas LYDC 47-23-30 revealed the highest value (1.74 $\Omega\,cm^2$) at 800 °C (Fig. 2a). This suggests that the relative volume ratio of conjugated YSZ with respect to YSZ core particles plays a critical role in the formation of a desirable cathode microstructure in terms of TPB formation and

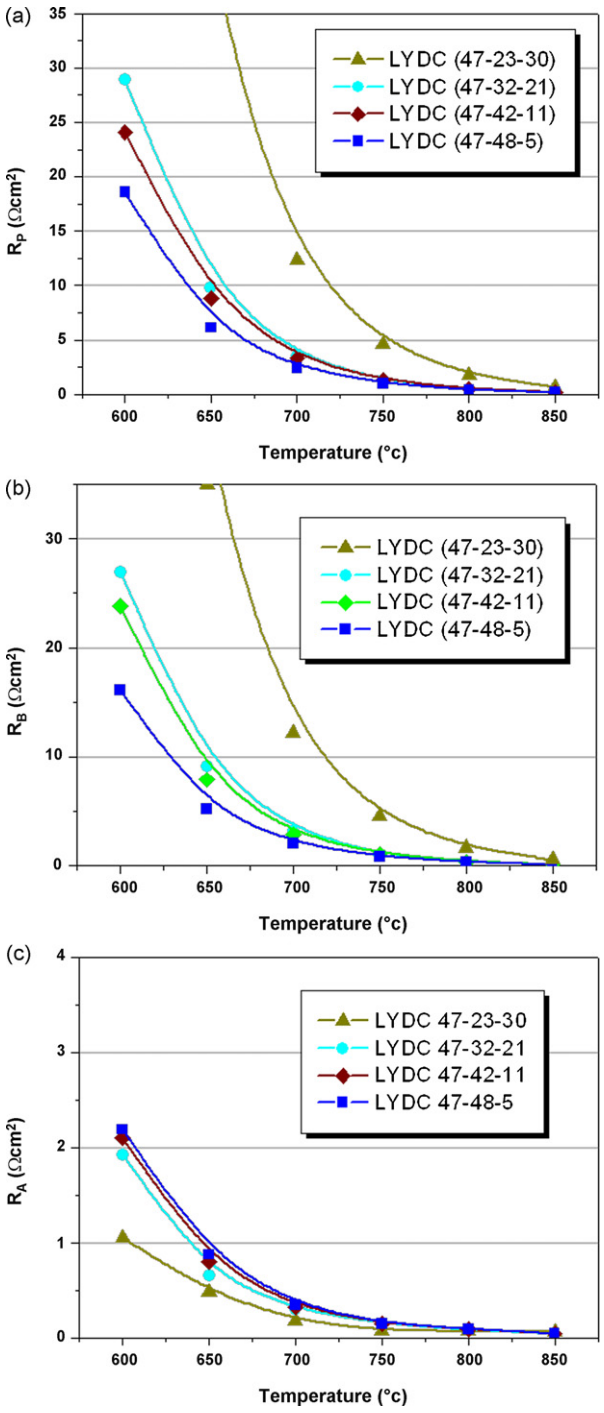

Fig. 2. Interfacial polarization resistances for symmetrical cells with four different LSM–YSZ compositions: (a) total interfacial polarization (R_P) resistance of composite cathodes where $R_P = R_A + R_B$, (b) polarization resistance of *process A* (R_A), (c) polarization resistance of *process B* (R_B). Impedance spectra obtained in air as function of cell operating temperature (600–850 °C).

YSZ connectivity. As shown in Fig. 2b, R_B decreases on reduction of the volume ratio of conjugated YSZ from 30 to 5 vol%, indicative of the formation of more TPB sites. By contrast, YSZ phase connectivity is improved by increasing the amount of conjugated YSZ phase from 5 to 30 vol%, as indicated by reduced R_A (Fig. 2c). These observations suggest that a composite cathode made from LYDC 47-23-30 would be durable because of a firm skeleton structure, but may suffer from less electrocatalytic activity due to reduced TPB sites.

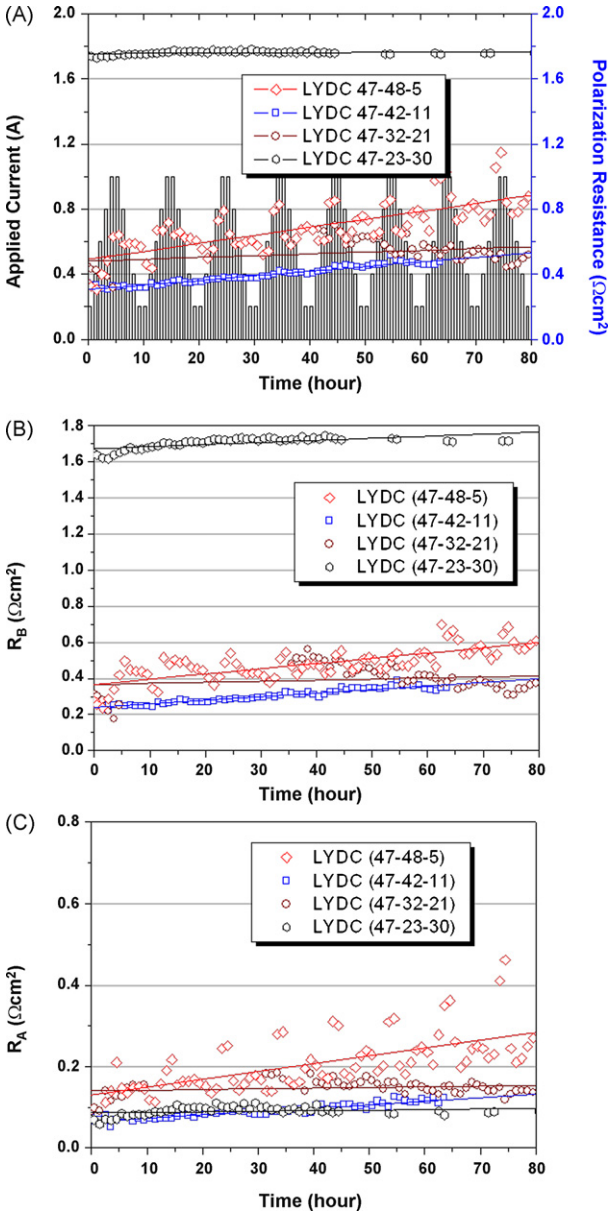

Fig. 3. Variation of area specific resistance of four different composite cathodes used in the symmetric cell configuration during accelerated life-time tests (ALT) at 800 °C: (a) total interfacial polarization resistance (R_P) and ALT profile, (b) polarization resistance for *process A* (R_A); (c) polarization resistance for *process B* (R_B).

Accelerated life-time testing was performed on the composite cathodes for rapid assessment their long-term stabilities [17]. Fig. 3 shows variations in the resolved interfacial polarization resistance during ALT at 800 °C for cells with four different composite cathodes. The total interfacial polarization resistances (R_P) for the cells with LYDC 47-48-5, 47-42-11, 47-32-21 and 47-23-30 cathodes at the initial stage were 0.344, 0.347, 0.445 and 1.72 Ω cm^2, respectively. The resistance of LYDC 47-23-30 was much higher than the other cathodes, although its resistance was constantly maintained until the end of the test. It was also noted that the electrode polarization of LYDC 47-32-21 was slightly higher than that of cathodes containing lower conjugated YSZ contents; but, its R_P value remains almost unchanged (0.51 Ω cm^2) even after 80 h of cyclic current stress, whereas the R_P values for 47-42-11 and 47-48-5 rise to 0.518 and 0.88 Ω cm^2, respectively. In addition, both the resolved resistance components of R_B and R_A increase during

the 80 h of accelerated testing, as shown in Fig. 3b and c, respectively. The percent increase for R_A (with respect to the initial value) is 5.67, 10, 81 and 121% as the volume fraction of conjugated YSZ is decreased from 30, 21, 11 to 5 vol%, whereas the corresponding percent increase for R_B is 4.4, 13.8, 64.4 and 69%. Considering the magnitude of the resistance variations, the relative amount of conjugated YSZ with respect to the YSZ core influences the YSZ phase interconnectivity more significantly than the TPB length. It is likely that the presence of conjugated YSZ nanoparticles enables the composite cathode to exhibit a strong microstructure due to enhanced YSZ connectivity. Based on the ALT results, the long-term stability of LYDC 47-23-30 is the best among the samples, but its polarization resistance is too high to be useful. The composite cathode made from LYDC 47-32-21 exhibits better long-term thermochemical and electrochemical stability compared with the other cathodes, while having a reasonably low polarization resistance. Also, it should

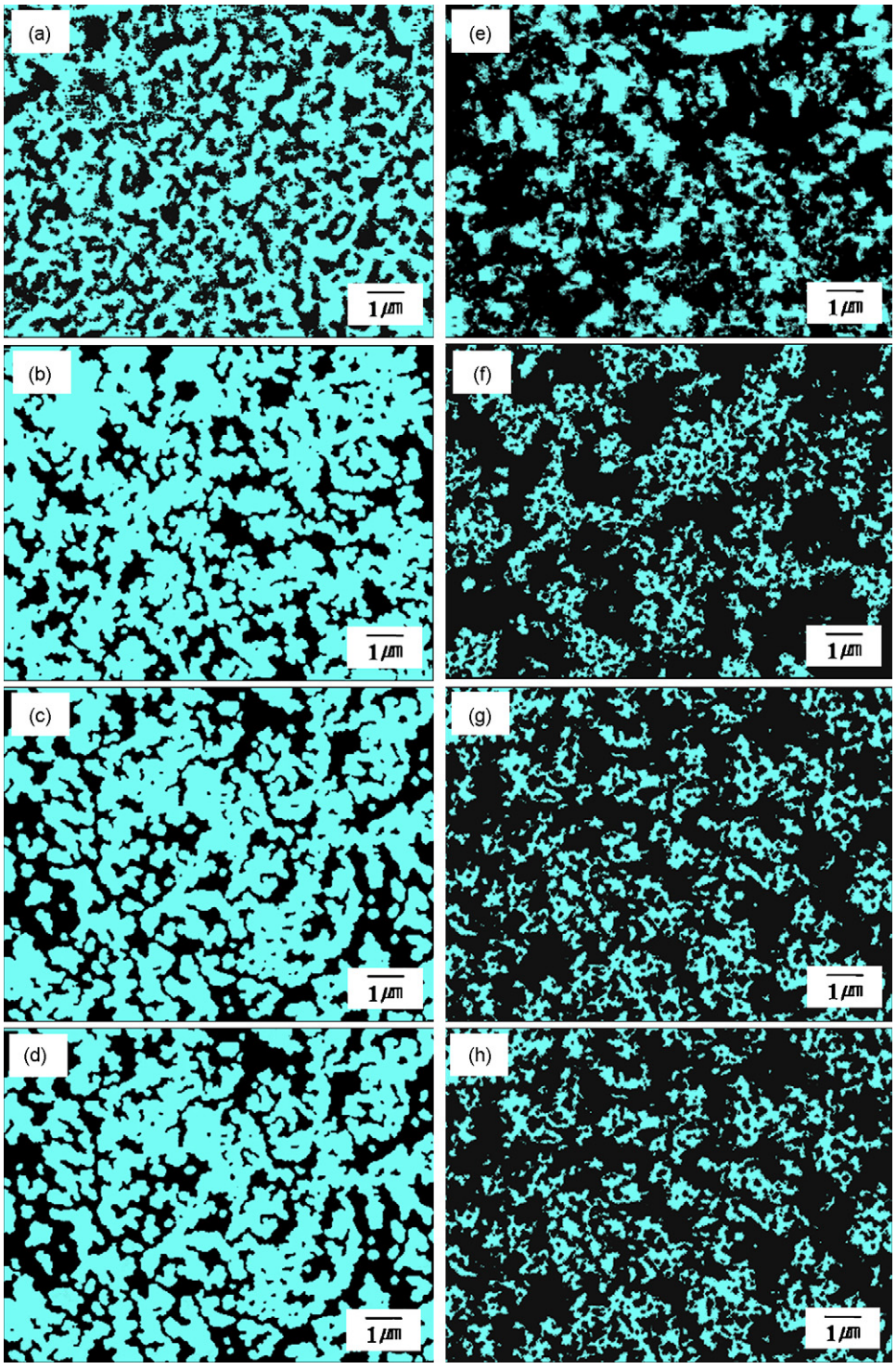

Fig. 4. SEM images of composite cathodes sintered at 1100 °C with different dual composite compositions: (a) polished and (e) LSM etched LYDC 47-23-30; (b) polished and (f) LSM etched LYDC 47-32-21; (c) polished and (g) LSM etched LYDC 47-42-11; (d) polished and (h) LSM etched LYDC 47-48-5.

Table 1
YSZ phase contiguity of LYDCs with different composite compositions.

Cathode type	47-48-5	47-42-11	47-32-21	47-23-30
Phase contiguity	0.44	0.48	0.52	0.69
Porosity (%)	41.1	40.1	41.2	39.5

be noted that use of the initial polarization resistances obtained from a simple half-cell test without ALT would be misleading in the determination of the optimal composition. To obtain a better understanding of the role of the conjugated YSZ, microstructural investigations were conducted as a function of cathode composition.

Panels a–d of Fig. 4 show binary images of cross-sectional views of fractured composite cathodes prepared with different compositions. All of the composite cathodes have approximately 40% porosity as determined by image analysis based on the SEM images (Table 1). The particles are well-connected, not only with each other but also with the electrolyte layer, for all of the composite cathodes. The influence of cathode composition on the electrode microstructure is difficult to recognize from simple fractured surface. Accordingly, binary images of the YSZ skeleton and pore structures were obtained after etching away the LSM phase. More detailed microstructural parameters such as YSZ phase contiguity can then be calculated using quantitative stereological theory [18,19]. Panels e–h of Fig. 4 present the YSZ skeleton structures of the cathodes with varying compositions. Different YSZ skeleton structures are observed as a function of volume ratio of conjugated YSZ with respect to the YSZ core. As summarized in Table 1, the phase contiguity value decreased continuously as the amount of conjugated YSZ phase is decreased. When the volume fraction of conjugated YSZ is higher than the YSZ core (i.e., 30 vol% conjugated YSZ), large YSZ grains are observed and the resulting YSZ phase has a thick skeleton structure as shown in Fig. 4e, in which the YSZ phase contiguity is characterized at 0.69. The decrease in the volume fraction of conjugated YSZ effectively breaks apart the phase connection and reduces the thickness of inter-grain necking. A further decrease from 11 to 5 vol% produces a less interconnected fine grain structure with some isolated grains, as shown in Fig. 4 h (contiguity = 0.44).

These observations correlate well with the corresponding resolved resistance data (see Fig. 3). The cathode with a smaller increase of R_A during ALT reveals a higher YSZ phase contiguity. The conjugated YSZ-added composite cathode characterized by the highest phase contiguity value (0.69) exhibits the lowest percent increase in R_A (5.67%). This indicates that a stable and firm YSZ skeleton structure fabricated using a higher content of conjugated YSZ provides for mechanical and electrochemical long-term stabilities. The R_B values also decrease with decreasing content of conjugated YSZ (i.e., decreasing phase contiguity). The composite cathode with 5 vol% conjugated YSZ has the lowest R_B, but experiences the largest increase of R_B during ALT. A less interconnected fine YSZ grain structure provides intimate contact with LSM phases and this results in enhanced LSM–YSZ contact points, i.e., TPB sites. On the other hand, the initial high cathodic performance degrades significantly during ALT because a less interconnected/isolated fine YSZ skeleton is incapable of preventing grain growth and/or coarsening of the LSM phase. In this respect, the R_B values for LYDC 47-32-21 and 47-23-30 are practically constant, while the R_B values of LYDC 47-42-11 and 47-48-5 increase to 64.4% and 69%. The use of a lower amount of the conjugated YSZ phase enables the formation of a highly electrochemically active cathode, but with a loss in long-term stability at the same time.

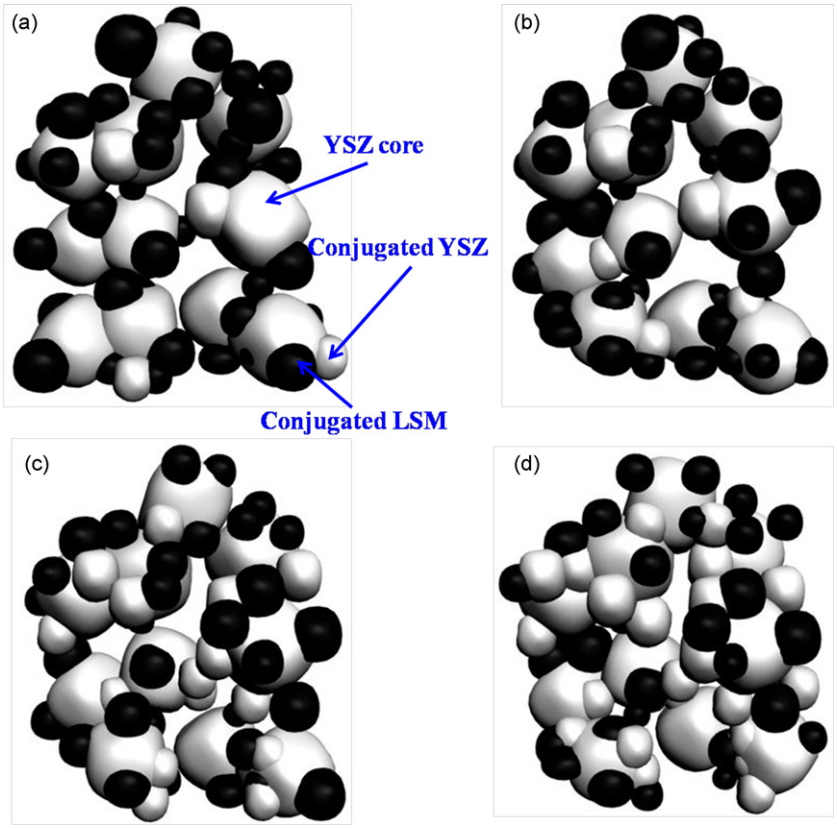

Fig. 5. Schematic illustrations of dual composite cathodes with different compositions: (a) LYDC 47-48-5, (b) LYDC 47-42-11, (c) LYDC 47-32-21, (d) LYDC 47-23-30.

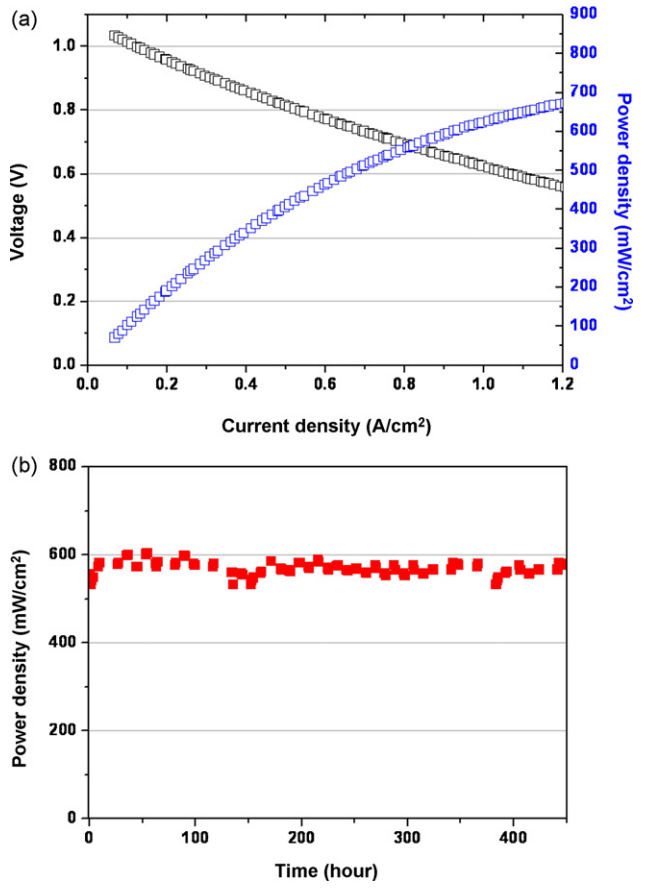

Fig. 6. Electrochemical performance of fuel cells based on LYDC 47-32-21 cathode: (a) cell performance and (b) power density variation at 0.7 V during a 500-h accelerated life-time test.

The role of conjugated YSZ nanoparticles with respect to the YSZ core nanoparticles can be clarified by a simple particle mixture model. A calculation was made of the number of conjugated LSM and YSZ particles per core particle of a given size in a unit cathode volume for a given dual composite composition. Considering the size ratio of the conjugated-to-core particles and the number ratio of conjugated LSM and YSZ particles as an attachment probability, the number of each of the conjugated particles necessary to surround a YSZ core particle can be estimated. The number of conjugated YSZ particles per YSZ core is 0.4, 1.0, 2.7 and 4.24 for the LYDC 47-48-5, 47-42-11, 47-32-21 and 47-23-30 cathodes, respectively. By contrast, the number of conjugated LSM particles per YSZ core is 4.01, 4.58, 6.01 and 6.65 for the LYDC 47-48-5, 47-42-11, 47-32-21 and 47-23-30 cathodes, respectively. If the conjugated YSZ nanoparticles act as interconnecting bridges between the YSZ core particles by which the YSZ backbone structure forms, the presence of more conjugated YSZ nanoparticles per YSZ core particle ensures a well-interconnected, and strong YSZ skeleton (i.e., lower increase of R_A and higher phase contiguity), resulting in a durable composite electrode. On the other hand, this reduces the probability of contact between LSM and YSZ core particles and in turn disturbs the formation of TPB sites (i.e., higher R_B) in the composite cathode. This hypothesis is illustrated in Fig. 5, which includes schematics of the particle mixture model. Panels a–d in Fig. 5 correspond to dual composite cathodes with compositions of 5, 11, 21 and 30 vol% conjugated YSZ nanoparticles, respectively. YSZ core particles should be surrounded by sufficient numbers of both conjugated LSM and YSZ phases to produce a well-connected YSZ skeleton structure, as well as to create the TPB sites. The dual composite model based on our calculations reveal that the LYDC 47-32-21 dual composite maintains balanced contact points between the conjugated YSZ/YSZ core and the conjugated LSM/YSZ core. From this point of view, LYDC 47-32-21 can be considered a good candidate for a very durable and high-performance composite cathode, which is also in good agreement with the experimental observations (Figs. 2 and 3).

Full-cell performances of LYDC 47-32-21 (cathode)/YSZ (electrolyte)/Ni-YSZ (anode) cells were investigated using humidified hydrogen. Fig. 6a shows the discharge profiles of the cells at 800 °C. The open-circuit voltage (OCV) is about 1.09 V. A maximum power density of ~680 mW cm^{-2} is observed at a current density of 1.2 A cm^{-2}. Fig. 6b shows the power density variation at 0.7 V as a function of accelerated testing time at 800 °C for the cells with the LYDC 47-32-21 cathode. The initial power densities of the cells with the 47-32-21 cathodes are ~549 mW cm^{-2}. The cells exhibit power improvement after 4 h, possibly due to electrochemically induced electrode activation [20]. The cell power density then remains nearly constant over 450 h, demonstrating its durability under cyclic current stress.

4. Conclusions

The influence of composition on the electrochemical performance and durability of LSM–YSZ dual composite cathodes has been examined. The dual composite cathodes consist of LSM and YSZ nanoparticles conjugated on large YSZ core particles. The use of both types of particle allows the development of an ideal cathode microstructure with improved phase contiguity and electrochemical activity. In particular, the volume fraction of the conjugated YSZ phase with respect to the YSZ core plays a critical role in maintaining electrode durability, while still exhibiting good cell performance. The amount of conjugated YSZ phase needs to be optimized: above the optimum levels for conjugated YSZ, the cathodes show durability but high polarization resistance; below the optimal levels for conjugated YSZ, the cathodes have low polarization resistance yet are unstable during high-temperature operations. The YSZ core particles should be surrounded by sufficient numbers of both conjugated LSM and YSZ nanoparticles to constitute a well-interconnected YSZ skeleton, as well as to create the enhanced TPB sites. Microstructural observations combined with impedance analysis confirm that a composition ratio of 47:32:21 vol% conjugated LSM:YSZ core:conjugated YSZ is optimum and that a cell with such a composition shows long-term durability in electrochemical performance.

Acknowledgements

This work was the outcome of the fostering project of the Specialized Graduate School of Hydrogen and Fuel Cells and was financially supported by the Ministry of Commerce, Industry and Energy (MOCIE) and the Seoul R&BD Program (CS070157). The study was also partially supported by the Korea Science and Engineering Foundation (KOSEF) through the National Research Laboratory. Program funded by the Ministry of Science and Technology (no. R0A-2005-000-10011-0).

References

[1] S. Singhal, K. Kendall, High-temperature solid oxide fuel cells: fundamentals, in: Design and Applications, Elsevier, Oxford, 2003, 73.
[2] E. Ivers-Tiffee, Q. Weber, D. Herbstritt, J. Eur. Ceram. Soc. 21 (2001) 1805–1811.
[3] M. Mogensen, S. Skaarup, Solid State Ionics 86–88 (1996) 1151–1160.
[4] T.Z. Sholklapper, V. Radmilovic, C.P. Jacobson, S.J. Visco, L.C. De Jonghe, Electrochem. Solid-State Lett. 10 (2007) B74–B76.

[5] E. Ivers-Tiffee, A. Weber, K. Schmid, V. Kerbs, Solid State Ionics 102 (2004) 223–232.
[6] M. Kuznecov, P. Otschik, P. Obenaus, K. Eichler, W. Schaffrath, Solid State Ionics 157 (2003) 371–378.
[7] T.Z. Sholklapper, H. Kurokawa, C.P. Jacobson, S.J. Visco, L.C. De Jonghe, Nano Lett. 7 (2007) 2136–2141.
[8] M. Kakihana, M. Arima, M. Yoshimura, N. Ikeda, Y. Sugitani, J. Alloys Compd. 283 (1999) 102–105.
[9] S.-D. Kim, H. Moon, S.-H. Hyun, J. Moon, J. Kim, H.-W. Lee, J. Power Sources 163 (2006) 392–397.
[10] H.S. Song, S.H. Hyun, J. Kim, H.-W. Lee, J. Moon, J. Mater. Chem. 18 (2008) 1087–1092.
[11] H.S. Song, W.H. Kim, S.H. Hyun, J. Moon, J. Kim, H.-W. Lee, J. Power Sources 167 (2007) 258–264.
[12] M.J. Jorgensen, M. Mogensen, J. Electrochem. Soc. 148 (2001) A433–A442.
[13] E.M. Skou, T. Jacobsen, Appl. Phys. A 49 (1989) 117–121.
[14] J. Fleig, P. Pham, P. Sztulzaft, J. Maier, Solid State Ionics 113–115 (1998) 739–747.
[15] M.J.L. Østergard, M. Mogensen, Electrochim. Acta 38 (1993) 2015–2020.
[16] Y.D. Zhen, S.P. Jiang, J. Electrochem. Soc. 153 (2006) A2245–A2254.
[17] W. Nelson, Accelerated life testing: statistical models, in: Test Plans and Data Analysis, John Wiley & Sons, New York, 1990, pp. 1–51.
[18] D. Simwonis, F. Tietz, D. Stoever, Solid State Ionics 132 (2000) 241–251.
[19] K.-R. Lee, S.H. Choi, J. Kim, H.-W. Lee, J.-H. Lee, J. Power Sources 140 (2005) 226–234.
[20] S. Koch, M. Mogensen, P.V. Hendriksen, N. Dekker, B. Rietveld, Fuel Cells 6 (2006) 117–122.